Challenge Journal of CONCRETE RESEARCH LETTERS

Research Article

Experimental study on the effect of polypropylene fiber on bond behavior, corrosion resistance, and microstructural characteristics of high-strength flowable concrete

Komala Nandaraju [a,*], Ramalingam Mourougane [a]

[a] *Department of Civil Engineering, Ramaiah Institute of Technology, Bengaluru 560054, Karnataka, India*

ABSTRACT

This study experimentally assesses the effects of polypropylene fibers (PPFs) on the mechanical, bond, durability, and microstructural performance of high-strength concrete (HSC) and high-strength flowable concrete (HSFC). A total of six M70-grade concrete mixes, with a characteristic compressive strength of 70 N/mm^2 at 28 days, were prepared: three HSC mixes and three HSFC mixes containing PPF at volume fractions of 0%, 0.1%, and 0.2%. Mechanical performance was evaluated through compressive, splitting tensile, and flexural strength tests at 3, 7, and 28 days. Bond behavior was examined using pull-out tests on deformed steel bars, while corrosion resistance was assessed using accelerated electrolytic corrosion testing. Microstructural changes during hydration were characterized by X-ray diffraction (XRD) and Fourier-transform infrared spectroscopy (FTIR). The results show that PPF improves tensile, flexural, and bond strength, with an optimum volume fraction of approximately 0.1%. The HSFC mixes exhibited slightly better post-cracking performance and bond strength than the HSC mixes, which can be attributed to more uniform fiber distribution and a denser matrix. Accelerated corrosion tests indicated that the fiber-reinforced mixes experienced lower steel mass loss and delayed crack initiation. XRD and FTIR analyses confirmed ongoing hydration and increasing microstructural density over time. The measured bond strengths exceeded the values predicted by IS 456:2000 and BS 8110, indicating that these code provisions are conservative for the studied fiber-reinforced high-strength concretes.

ARTICLE INFO

Article history:
Received – January 9, 2026
Revision requested – February 12, 2026
Revision received – March 11, 2026
Accepted – March 28, 2026

Keywords:
High-strength concrete
Microstructural characterization
Accelerated corrosion
Bond behavior
Polypropylene fibers

Citation: Nandaraju K, Mourougane R (2026). Experimental study on the effect of polypropylene fiber on bond behavior, corrosion resistance, and microstructural characteristics of high-strength flowable concrete. *Challenge Journal of Concrete Research Letters*, 17(2), 147–161.

1. Introduction

Plain concrete and reinforced concrete (RC) are widely used in civil engineering because of their strength, stiffness, cost efficiency, and suitability for various structural applications. Fig. 1 summarizes the main performance-related properties of concrete. However, the increasing use of cement-based materials has raised sustainability concerns related to Portland cement production, encouraging the incorporation of supplementary cementitious materials and industrial by-products as partial binder replacements (Mohamad et al. 2025; Tanash et al. 2025). At the same time, the long-term performance of RC structures is often limited by deterioration mechanisms such as reinforcement corrosion, drying shrinkage, and cracking, which may reduce load-carrying capacity and shorten service life. In this context, high-strength concrete (HSC) and high-strength flowable concrete (HSFC) have been developed to provide higher load capacity, improved durability, and better construction efficiency, particularly in structural members where dense reinforcement, bond performance,

* *Corresponding author*. E-mail address: komala.n@msrit.edu (K. Nandaraju)
ISSN: 2548-0928 / DOI: https://doi.org/10.20528/cjcrl.2026.02.006

and resistance to aggressive environments are critical. The high compressive strength of HSC, which is achieved by using very low water-to-binder ratios and developing dense microstructures, is far greater than that of conventional concrete (Hasan et al. 2025; Torres-Ortega et al. 2021). However, the dense microstructure and high strength of HSC may reduce workability, making placement and compaction more difficult in heavily reinforced or complex formwork (De Alencar Monteiro et al. 2018; Mazaheripour et al. 2011). HSFC addresses these workability limitations through high-range water-reducing admixtures, supplementary cementitious materials, and fine-particle packing, which together produce a flowable and self-compacting mix without vibration (Abdraimov 2024; Mazaheripour et al. 2011; Uysal and Tanyildizi 2012).

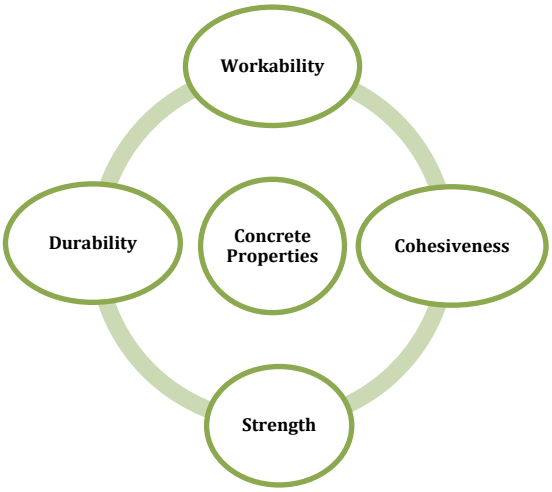

Fig. 1. Main properties of concrete.

PPFs are increasingly used in HSC and HSFC to improve tensile resistance, post-cracking behavior, crack control, and energy absorption (De Alencar Monteiro et al. 2018; Khaloo et al. 2022; Qin et al. 2019; Resende et al. 2022). Their low elastic modulus, chemical stability, and high elongation capacity allow properly dosed PPFs to bridge microcracks and improve ductility without causing a substantial reduction in compressive strength or fresh-state performance. This effect is particularly important in high-strength and flowable concrete systems, where dense matrices provide high strength but may also increase brittleness and create placement difficulties in heavily reinforced or complex structural members.

The performance of PPF-reinforced HSC and HSFC is also strongly influenced by the binder system and mixture proportioning. When PPFs are combined with mineral admixtures, nano-additions, or pozzolanic industrial by-products, these additions can improve strength, refine the pore structure, promote additional hydration products, increase durability, and help maintain adequate workability when used at suitable dosages (Abdraimov 2024; Al-Safi et al. 2025; Hasan et al. 2025; Mohamad et al. 2025; Srivastava et al. 2025; Tanash et al. 2025; Uysal and Tanyildizi 2012). However, excessive replacement levels, unsuitable particle dispersion, or increased water demand may reduce workability, increase porosity, and weaken fiber-matrix interaction, indicating that mixture proportioning remains critical for fiber-reinforced high-strength systems (Mohamad et al. 2025; Srivastava et al. 2025; Tanash et al. 2025). Previous studies have also shown that the use of PPF in self-compacting or flowable concrete can affect slump flow, passing ability, viscosity, and superplasticizer demand, especially when mineral additives, micro-silica, or alternative fine aggregates are incorporated into the mixture (Abdraimov 2024; Dubal and Naktode 2024; Mazaheripour et al. 2011; Uysal and Tanyildizi 2012).

Previous research further indicates that PPF and hybrid fiber systems can improve fracture resistance, deformability, residual load capacity, ductility, post-peak behavior, and crack control in high-strength concretes (Bakhita et al. 2025; De Alencar Monteiro et al. 2018; Hima Bindu et al. 2024; Khaloo et al. 2022). Under elevated temperature or other severe exposure conditions, PPF has been reported to reduce explosive spalling, support residual mechanical performance, and contribute to strength retention, while fiber type and post-exposure treatment can further influence the recovery and durability of fiber-reinforced concretes (Resende et al. 2022; Urtekin and Çelik 2025; Zhao et al. 2022). In addition, recycled polypropylene particles and combined fiber-SCM systems have been associated with improved sustainability, chloride resistance, microstructural densification, and cost-effective crack control (Faraj et al. 2019; Hasan et al. 2025; Labaran et al. 2024). Overall, these findings support the use of PPF-reinforced HSC and HSFC in structural applications where mechanical performance, durability, bond behavior, and resistance to aggressive environments are required.

1.1. X-ray diffraction (XRD) and Fourier-transform infrared spectroscopy (FTIR) analysis

Microstructural characterization methods such as XRD and FTIR are increasingly used as complementary tests alongside mechanical and durability assessments of advanced concretes. These techniques provide information on hydration phases, crystalline and amorphous contents, and chemical interactions among fibers, the cement matrix, and supplementary cementitious materials (SCMs) (Hasan et al. 2025; Resende et al. 2022). XRD analysis identifies crystalline hydration products, such as portlandite ($Ca(OH)_2$), ettringite, and calcium silicate hydrate (C-S-H), as well as secondary phases associated with SCMs such as silica fume or nano-silica additions (Abdraimov 2024; Hasan et al. 2025). In PPF systems, XRD can reveal changes caused by high-temperature exposure or fiber addition that may alter hydration rates or lead to decomposition or dehydration of phase-transition products. At elevated temperatures, XRD patterns have indicated phase changes such as portlandite decomposition and the transformation of C-S-H zones into more crystalline transitional phases, which are related to residual-strength changes (Resende et al. 2022; Zhao et al. 2022).

In fiber-reinforced HSC and HSFC, FTIR spectra typically show prominent peaks corresponding to Si-O stretching in the C-S-H gel phase, hydroxyl groups associated with portlandite, and carbonate ($CaCO_3$) formed

through carbonation. Combined microstructural and fracture-property analyses show how PPF affects crack networks at the micro-level (Torres-Ortega et al. 2021). Therefore, changes in the intensity or position of these peaks can indicate modifications in hydration products caused by fiber inclusion, SCM content, or environmental exposure. For example, Resende et al. (2022) showed that FTIR can detect signals related to polymer degradation and changes in cement-matrix chemistry after thermal loading, confirming the onset of polypropylene melting and the associated microstructural changes. Hasan et al. (2025) reported that FTIR observations, together with mineralogical densification detected by XRD and increased resistance to chloride penetration, support improved durability at higher SCM contents. Thus, combined XRD, FTIR, mechanical, and durability results can provide a more comprehensive understanding of the performance mechanisms of HSC and HSFC.

The bond behavior between reinforcing steel and concrete is crucial because it enables composite action and transfers stress between the two materials. Loss of bond performance directly affects crack spacing, deflection, anchorage length, and ultimately structural integrity. Bond degradation is influenced by the physical and mechanical properties of the reinforcing steel and concrete, environmental exposure, and time-dependent deformations caused by drying, corrosion-induced expansion, and shrinkage.

Fiber reinforcement is an effective approach for improving the strength, durability, and post-cracking behavior of concrete. Fibers bridge cracks after their formation, provide additional confinement around reinforcing bars, and can therefore influence the bond between steel reinforcement and the surrounding concrete (Ranjbar et al. 2016; Varghese et al. 2019). Pull-out-based studies have also shown that bond resistance and stress transfer are strongly affected by matrix composition, fiber surface condition, and interfacial compatibility, even in different fiber-reinforced cementitious or earth-based composite systems (Tarhan et al. 2025). In reinforced concrete, both metallic and non-metallic fibers have been reported to increase bond strength and delay splitting failure in pull-out tests (Deng and Yang 2024; Tsiotsias and Pantazopoulou 2021).

PPF, basalt, cellulose, and other synthetic fibers have gained attention because of their corrosion resistance, low density, and ability to control microcracking (Ahmed et al. 2021; Chen et al. 2024; Touahri et al. 2021). Experimental studies have shown that PPF helps retain bond strength under wet conditions by limiting cracking and maintaining support around the steel bar (Deng and Yang 2024; Ranjbar et al. 2016). Hybrid and coarse synthetic fibers are also being evaluated as possible replacements for steel fibers and have shown tensile and bond-strength performance comparable to that of high-performance and ultra-high-performance concrete, while offering durability and sustainability benefits (Lin et al. 2024; Sangkeaw et al. 2025).

The bond between reinforcing steel and concrete is essential for ensuring composite action and effective stress transfer in RC members. The bond between ribbed steel bars and the surrounding cementitious matrix depends on mechanical interlocking and friction between the bar ribs and the matrix (Diab et al. 2014; Tastani and Pantazopoulou 2010). Several factors influence bond performance, including concrete compressive strength, bar diameter, embedment length, bar surface deformation, and confinement type (Burdziński and Niedostatkiewicz 2022; Hadi 2008; Torre-Casanova et al. 2013). High-strength and high-performance concretes generally provide higher bond strength because of their dense microstructures and superior mechanical properties. However, they are also more susceptible to brittle splitting because of their lower deformation capacity (Hadi 2008; Tsiotsias and Pantazopoulou 2021). Previous studies have observed reductions in bond strength and shifts in pull-out failure modes as reinforcement corrosion increases. Accelerated corrosion tests further show that bond deterioration decreases peak bond strength and increases slip, thereby reducing structural ductility (Hou et al. 2019; Leporace-Guimil et al. 2021). Drying-shrinkage cracking also affects bond behavior because reduced confinement pressure around the reinforcing steel increases slip and decreases bond strength (Hou et al. 2019).

Corrosion of steel reinforcement is a major cause of premature deterioration in concrete structures, especially in environments with high chloride-ion concentrations, such as marine environments or structures exposed to de-icing salts. Chloride ions migrate through concrete and reach the steel reinforcement, where they damage the passive film and initiate electrochemical corrosion (Sola et al. 2019; Song and Saraswathy 2007). The volume of corrosion products exceeds that of the original steel, generating stresses in the surrounding concrete and leading to cracking, spalling, and reduced bond strength. Electrochemical methods allow the initiation and progression of corrosion in reinforced concrete to be detected through techniques such as half-cell potential measurements, corrosion-current-density measurements, and accelerated corrosion tests (Pan et al. 2020; Song and Saraswathy 2007). In addition to electrochemical techniques, acoustic emission monitoring has been used as a non-invasive method to detect corrosion-induced microcracking and to develop corrosion-rate prediction models based on recorded signal parameters (Patil 2025). These methods provide quantitative real-time information on corrosion activity and facilitate the evaluation of different concrete types, synthetic materials, fibers, SCMs, and corrosion inhibitors (Aguirre-Guerrero et al. 2021; Fahmy et al. 2022; Ouda 2024). Recent research shows that high-performance concrete and fiber-reinforced concrete can reduce corrosion rates and improve electrochemical performance by controlling cracking and refining pore structure, thereby limiting chloride transport (Bajić et al. 2025; Deng and Yang 2024; Leporace-Guimil et al. 2021). Nevertheless, corrosion-related bond deterioration remains critical when shrinkage cracking and sustained loading affect bond development (Hou et al. 2019). Fig. 2 illustrates the effects of PPF in hardened concrete.

Although fiber-reinforced concrete has been widely studied, most investigations treat mechanical behavior and durability as separate topics. Previous studies have examined the effects of PPF on tensile strength, flexural performance, and crack control, whereas other studies

have addressed corrosion resistance or microstructural properties using separate test methods. However, the relationships among mechanical performance, bond behavior, durability, and microstructural change remain insufficiently integrated. In addition, only a limited number of studies have directly compared HSC and HSFC reinforced with PPF under similar mix proportions. The improved workability of HSFC may influence fiber distribution and interfacial transition-zone properties, thereby affecting bond strength and corrosion resistance.

This study provides an integrated evaluation of mechanical properties, pull-out bond behavior, corrosion resistance, and microstructural characteristics using XRD and FTIR within the same experimental framework for both HSC and HSFC systems at identical fiber dosages. It also assesses bond-strength predictions according to BS 8110 (1997) and IS 456 (2000).

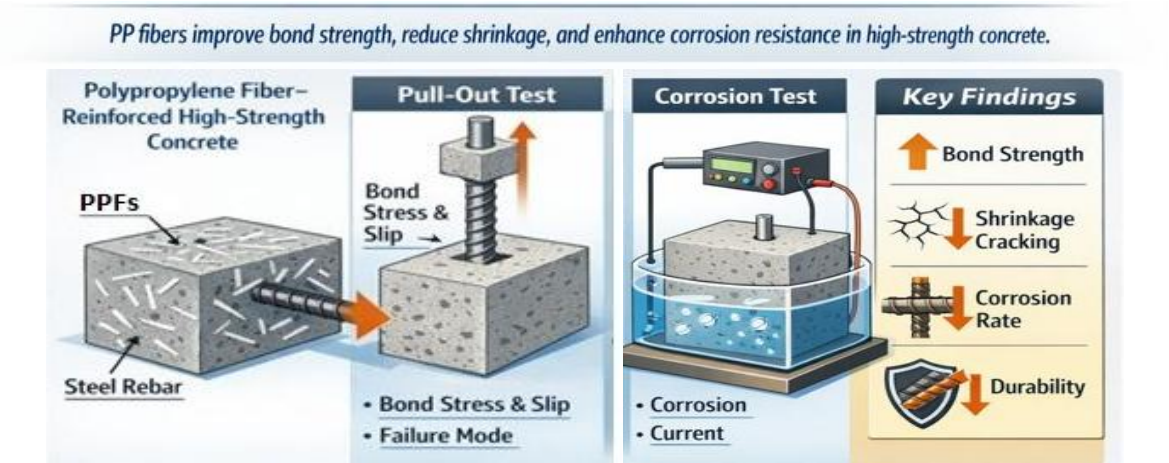

Fig. 2. Effects of PPF in pull-out and accelerated corrosion tests.

2. Research Gap and Novelty

Current research generally focuses on three separate areas: mechanical performance of PPF-reinforced HSC, corrosion resistance, and microstructural characterization. Direct quantitative comparisons between HSC and HSFC containing identical PPF dosages remain limited. Therefore, this study compares HSC and HSFC using the same fiber contents and evaluates mechanical, bond, corrosion, and microstructural responses within a single experimental framework.

The present study aims to:

- Compare the mechanical properties of HSC and HSFC containing identical PPF contents of 0%, 0.1%, and 0.2%.
- Examine the bond behavior between reinforcing steel and fiber-reinforced high-strength concrete using pull-out tests.
- Assess the corrosion resistance of reinforced concrete using an accelerated electrolytic corrosion test.
- Investigate microstructural changes using XRD and FTIR techniques.
- Evaluate the reliability of IS 456:2000 and BS 8110 predictions for bond strength in polypropylene-fiber-reinforced high-strength concrete systems.

3. Materials and Methods

The experimental program used 53-grade ordinary Portland cement (OPC) conforming to IS 12269 (2013), manufactured sand as fine aggregate, and crushed coarse aggregate with a maximum nominal size of 12.5 mm. The HSFC mixes contained both a superplasticizer and a viscosity-modifying agent (VMA), whereas the HSC mixes contained only a polycarboxylate ether (PCE)-based superplasticizer. Table 1 presents the physical properties of the synthetic micro-PPF used in this study. Fly ash and silica fume were used as SCMs; fly ash was incorporated at 15% by weight for HSC and 20% for HSFC, while silica fume was used at 5% by weight for both HSC and HSFC. Fig. 3 shows the materials used in concrete preparation. Concrete mix preparation was carried out in accordance with IS 10262 (2019), and six mixes were produced: three HSC mixes and three HSFC mixes with and without fibers. Basic material tests and fresh-property assessments were performed in accordance with the relevant standards, and all results were within acceptable limits. Mechanical performance was evaluated through compressive, splitting tensile, and flexural strength tests at 3, 7, and 28 days. Water absorption was measured in accordance with ASTM C1585 (2020). Microstructural analysis was conducted using XRD and FTIR after 28 days of curing.

Table 1. Physical properties of polypropylene fibers.

Property	Value
Shape	Triangular
Cut length	12 mm
Effective diameter	30 μm
Specific gravity	0.91
Melting point	160-165 °C
Elongation	90%
Young's modulus	4000 MPa

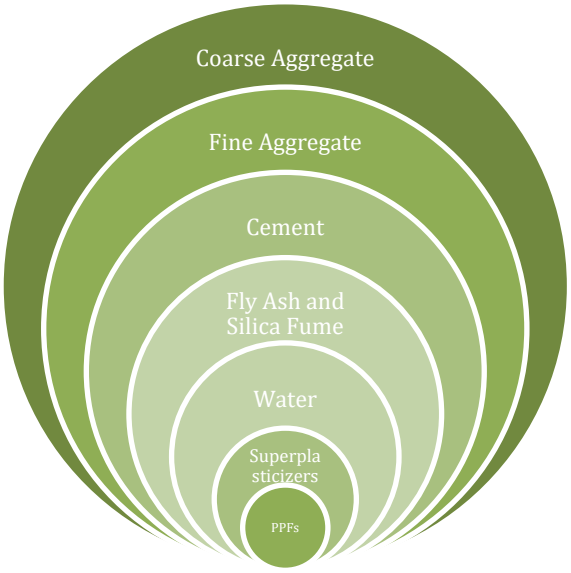

Fig. 3. Materials used in concrete preparation.

4. Experimental Work

4.1. Mechanical properties

The compressive, splitting tensile, and flexural strengths of HSC and HSFC with and without PPF were evaluated at 3, 7, and 28 days of curing for mixes M1-M6, as defined in Table 2. Compressive tests were performed on 100×100×100 mm cube specimens using a calibrated compression testing machine in accordance with IS 516 (1959). Splitting tensile strength was determined in accordance with IS 5816 (1999) using 100×200 mm cylindrical specimens subjected to diametral loading until failure. Flexural strength was assessed using a two-point loading setup on 75×75×450 mm prism specimens in accordance with IS 516 (1959). Fig. 4 illustrates the mechanical strength testing setup.

Table 2. Mix codes used in the study.

M1-HSC (0% PPF)	High-strength concrete
M2-HSC (0.1% PPF)	High-strength concrete
M3-HSC (0.2% PPF)	High-strength concrete
M4-HSFC (0% PPF)	High-strength flowable concrete
M5-HSFC (0.1% PPF)	High-strength flowable concrete
M6-HSFC (0.2% PPF)	High-strength flowable concrete

4.2. Accelerated corrosion test

To determine concrete resistance to corrosion, an accelerated electrolytic corrosion test was performed on specimens prepared from mixes M1-M6. Cylindrical specimens with a diameter of 100 mm and a height of 200 mm contained a 10 mm diameter steel bar at the center, providing a concrete cover of 45 mm, and were cured for 28 days, as shown in Fig. 5. The specimens were then submerged in a 5% sodium chloride solution, where the steel bar served as the anode and an external stainless-steel plate served as the cathode. The system was operated under direct current (DC), with voltage maintained throughout the test while current variations were monitored. Fig. 6 illustrates the testing procedure. Corrosion initiation was identified by a sudden increase in current and the appearance of visible surface cracks. After testing, the specimens were broken open, and the reinforcement bars were extracted, cleaned with Clark's solution, dried, and weighed to determine corrosion-related mass loss.

Fig. 4. Mechanical strength testing setup.

4.3. Pull-out bond strength test

To evaluate the bond strength between deformed reinforcing bars and concrete, pull-out tests were performed on specimens from mixes M1-M6. Each specimen consisted of a 150×150×150 mm concrete cube with a central 12 mm diameter deformed bar. The embedment length was 150 mm to ensure a consistent bond length during testing. After 24 h, the specimens were demolded and subjected to 28 days of water curing. Before testing, the protruding ends of the embedded bars were cleaned and prepared for placement in the mounting fixture, as shown in Fig. 7. The specimens were mounted in a 400 kN universal testing machine (UTM), which held the cubes securely while the bars were pulled axially from the concrete.

Fig. 5. Specimens used for accelerated corrosion testing during curing and after corrosion.

Fig. 6. Accelerated corrosion test setup.

Fig. 7. Test setup for pull-out test.

The steel bar was pulled at a constant loading rate of 0.5 mm/min until failure occurred by either bar slip or concrete splitting. At failure, the maximum applied load (P_{max}) was recorded. The average bond stress (τ_b) was calculated using Eq. (1).

$$\tau_b = \frac{P_{max}}{\pi d l} \quad (1)$$

where P_{max} is the peak pull-out load, d is the rebar diameter (12 mm), and l is the embedded length of the rebar (150 mm). This procedure follows the recommendations of IS 2770 (1967) for evaluating the bond performance of steel reinforcement in fiber-reinforced concrete.

5. Results and Discussion

5.1. Mechanical properties

All concrete mixtures achieved the characteristic strength of 70 MPa at 28 days, with ultimate compressive strengths ranging from 75.7 to 77.9 MPa for mixes M1-M6. Strength development followed a typical hydration pattern, with approximately 55-60% of the 28-day strength reached at 3 days and approximately 70-80% reached at 7 days. The addition of PPF caused only minor fluctuations in compressive strength, within approximately ±3%. A slight increase was observed at the 0.1% fiber dosage, which may be attributed to improved microcrack control and matrix integrity. At 0.2% PPF, the improvement was limited, possibly because of fiber agglomeration and reduced workability. The HSFC mixes showed slightly better performance than the HSC mixes, which may be related to better packing density and more uniform fiber distribution. Overall, PPF had a limited effect on compressive strength.

In the splitting tensile strength test, the control mix reached 5.7 MPa at 28 days, while 0.1% PPF increased the strength to 6.3-6.5 MPa, corresponding to an improvement of approximately 10-18%. The increase at 0.2% PPF was smaller but still noticeable. The improvement is attributed to crack-bridging action and stress redistribution, which enhance energy absorption. The HSFC mixes exhibited slightly higher tensile strength than the HSC mixes because of their superior fiber distribution and denser microstructure. Based on these results, the optimum fiber dosage was 0.1% by volume.

Flexural strength also improved in the HSC and HSFC mixes containing PPF. The control mixes reached 7.1-7.3 MPa at 28 days, while 0.1% PPF increased flexural strength to approximately 7.9 MPa, corresponding to an improvement of 8-12%. The increase at 0.2% PPF was less pronounced. The fibers improved crack resistance, post-cracking ductility, and toughness during bending. The HSFC mixes performed better than the HSC mixes because of improved fiber-matrix bonding and better structural integrity. Fig. 8 presents the mechanical strength test results.

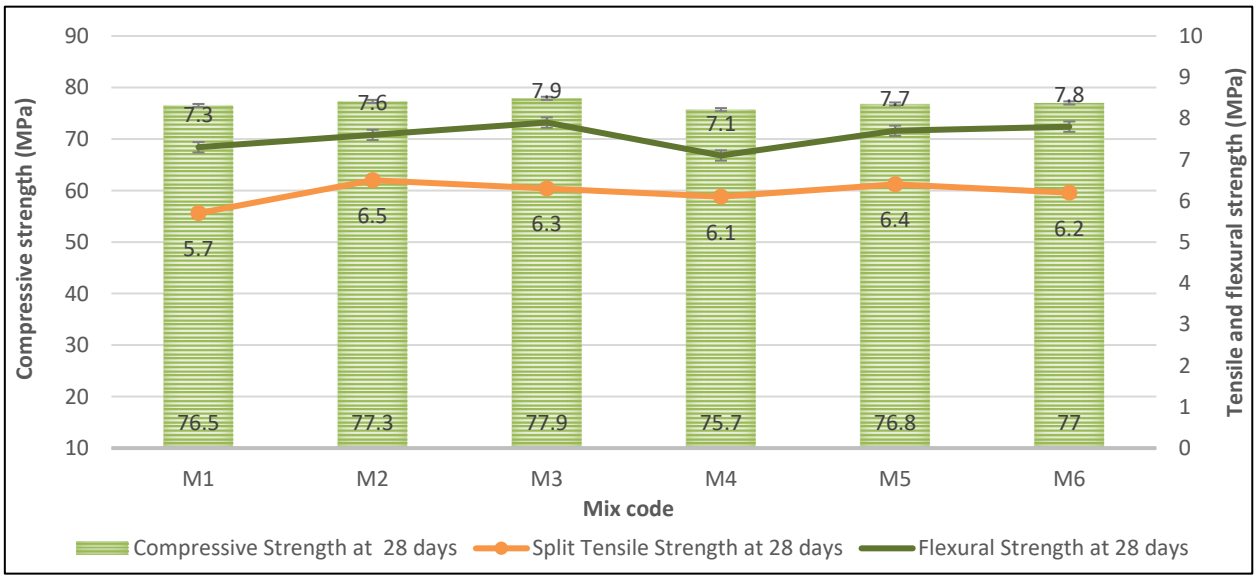

Fig. 8. Mechanical strength test results.

5.2. FTIR and XRD analyses

Fig. 9 shows the FTIR spectrum in the region of approximately 3640-3700 cm^{-1}, where the sharp band at about 3640 cm^{-1} is associated with O-H stretching of structural hydroxyl groups from portlandite or bound water in ettringite. The broad feature at about 3400 cm^{-1} and the bending mode at about 1650 cm^{-1} are associated with molecular water. The asymmetric stretching of carbonate ions (CO_3^{2-}) appears at about 1410-1480 cm^{-1}, with an out-of-plane bending mode at about 875 cm^{-1}. These bands increased in intensity from early to late samples, suggesting increased calcite formation. Bands related to S-O stretching in sulfate phases at about 1100-1130 cm^{-1} decreased over time as ettringite and gypsum were consumed during carbonation. The Si-O stretching modes at about 980-1000 cm^{-1} and Si-O-Si bending modes at about 450-500 cm^{-1} remained largely unchanged, confirming the non-reactive nature of quartz. The band at about 3400 cm^{-1} broadened at intermediate hydration stages, possibly because of increased hydroxyl disorder in hydroxyl-containing phases and bound wa-

ter, and then decreased toward the final stage. These spectral trends agree with the XRD results, where the ettringite peak diminished, calcite reflections increased from M1 to M6, sulfate bands decreased, and carbonate modes developed, indicating a more crystalline and carbonate-rich end product.

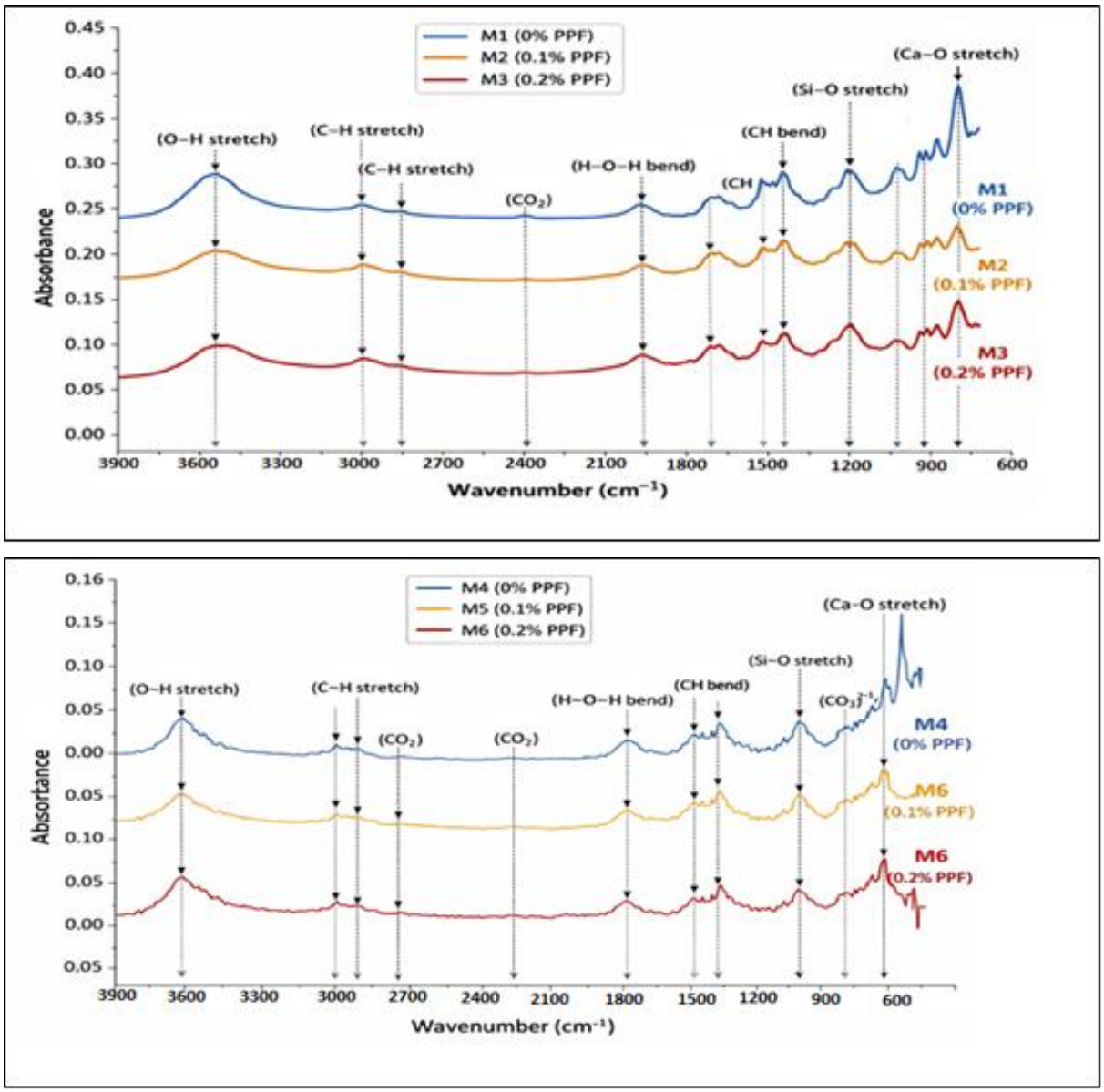

Fig. 9. FTIR analysis results.

The XRD data shown in Fig. 10 for phases M1-M6 indicate clear mineralogical evolution caused by carbonation or phase transformation in the stable samples.

The M1 and M5 specimens exhibited a quartz-dominated crystalline framework. Although this framework provides structural support, the limited development of hydration products may increase interfacial porosity and reduce bond strength. M3 showed reduced quartz intensity and the development of ettringite at approximately 10.3° and C-S-H between 29° and 35°, indicating advanced chemical conversion. The M2 group exhibited higher bond strength because ettringite needle growth and C-S-H gel formation occurred within the capillary pores. This mineralogical evolution enhanced mechanical interlocking at the reinforcement interface. FTIR analysis confirmed silicate polymerization, indicating the formation of a stronger binder matrix with improved resistance to pull-out forces compared with the siliceous matrix of M1. Electrochemical performance depends on the physical barrier provided by hydrated phases. M4 exhibited amorphous characteristics, resulting in a dense structure that blocked ionic diffusion through more complex pathways, as indicated by the absence of distinct crystalline peaks. This micro-densification delayed corrosion initiation. The presence of calcite in M6 indicates that carbonation may depassivate the embedded steel; thus, XRD can help evaluate the electrochemical stability of the reinforcement. Table 3 presents the XRD and FTIR results.

- Calcite formation resulted in pore refinement and reduced chloride transport.
- Reduced ettringite indicated stabilization of the matrix.
- Dense C-S-H improved the ITZ and increased bond strength.

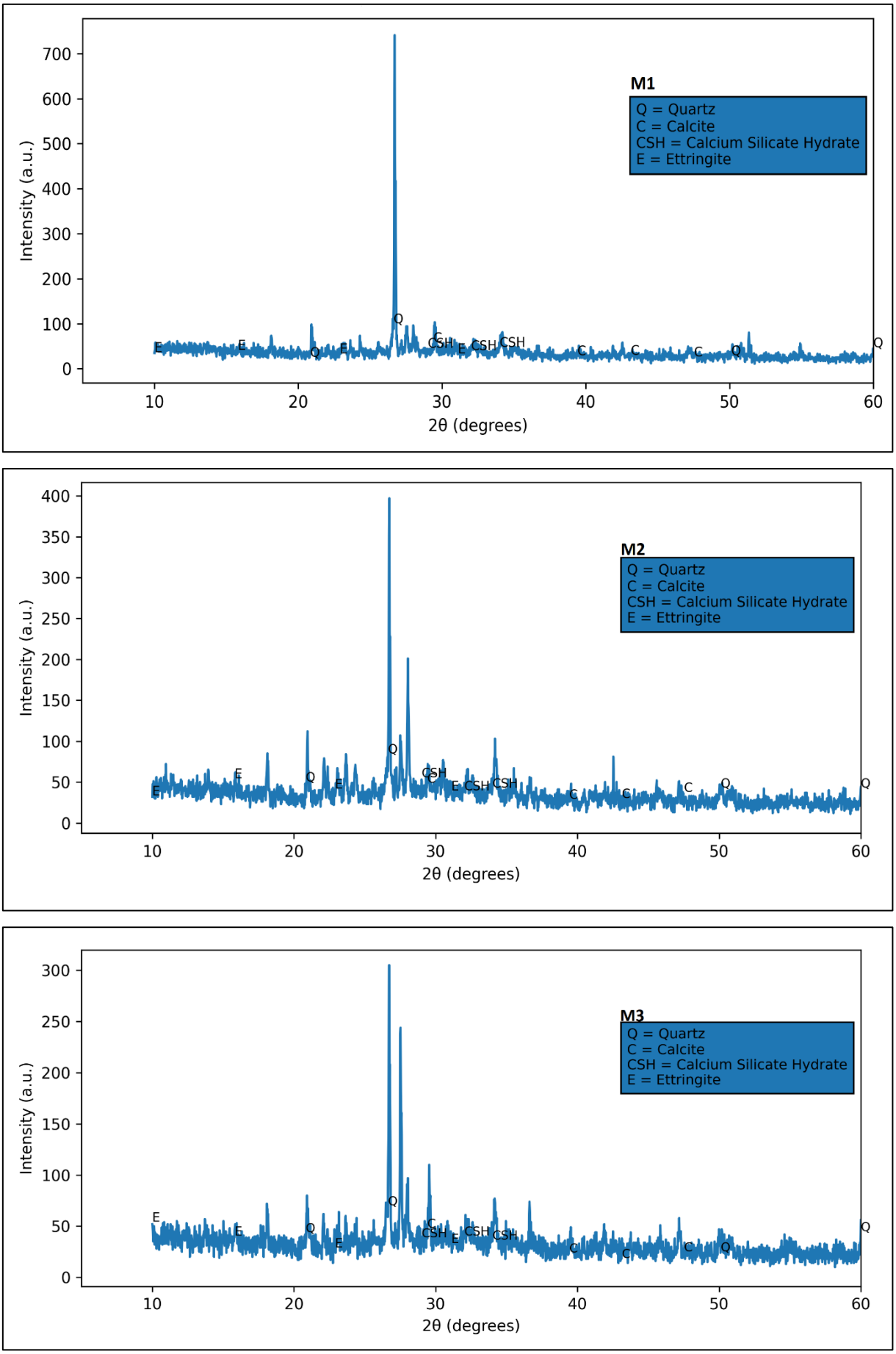

Fig. 10. (continued)

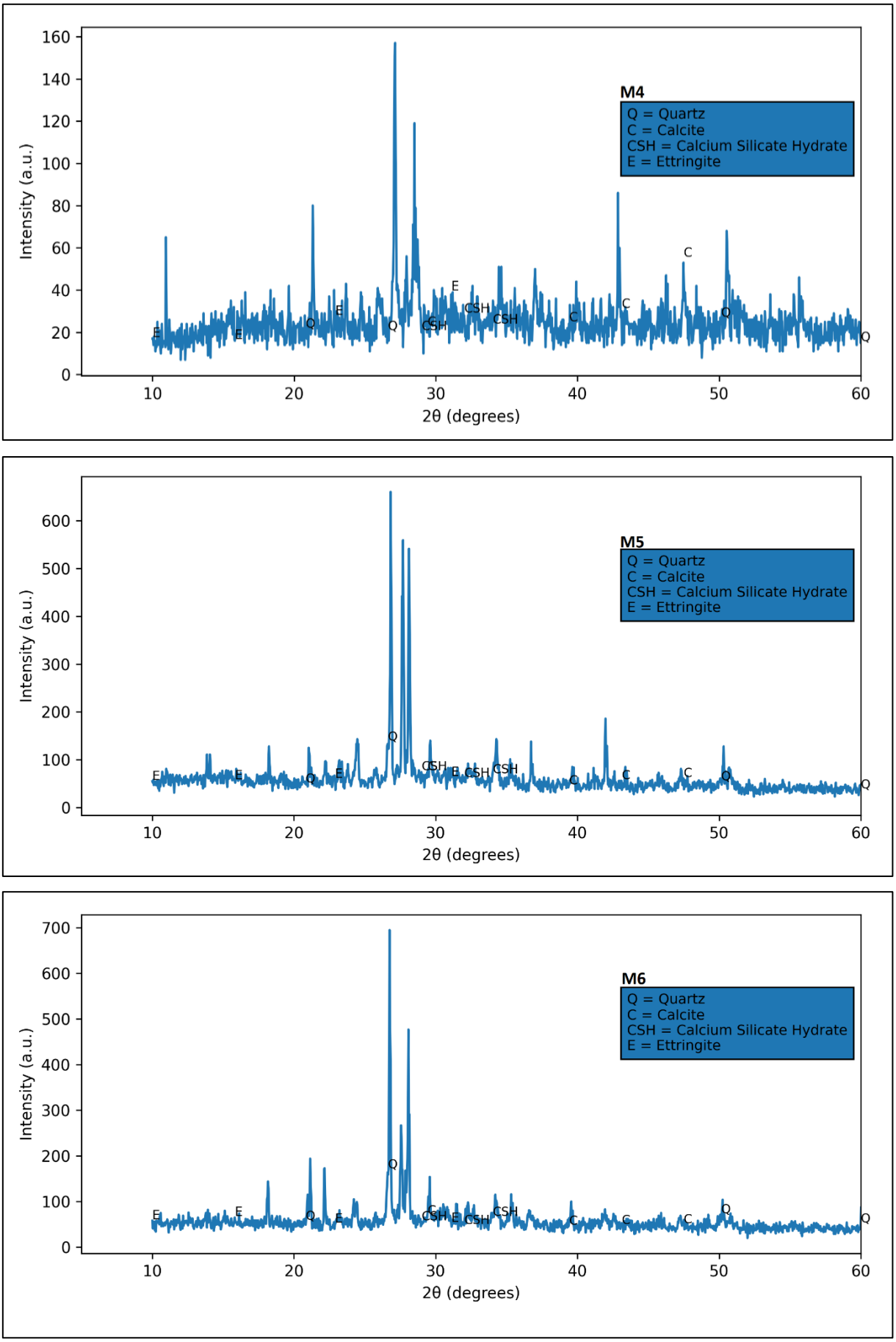

Fig. 10. XRD analysis results for M1-M6.

Table 3. XRD and FTIR analysis results.

Mix code	XRD points	FTIR points	Bond-strength mechanism	Corrosion-resistance basis
M1, M5	Quartz peaks with hydration products.	Low silicate polymerization indicated by the main Si-O stretching and Si-O bond-configuration bands.	The interfacial transition zone (ITZ) shows relatively weak mechanical interlocking because of its porous structure, limited C-S-H development, and the presence of less-reactive filler material.	Interconnected pores permit chloride-ion ingress because the hydration products do not sufficiently block pore pathways.
M2, M3	Main C-S-H diffraction pattern and ettringite-related diffraction pattern, together with vanadium oxide and silicate-based polymer materials.	High silicate polymerization indicated by silica-oxygen stretching and silicon-oxygen bond-stretching bands.	The fiber-concrete interface shows improved chemical adhesion and mechanical interlocking through the combined presence of dense C-S-H and ettringite.	The improved pore structure increases ionic tortuosity and electrical resistivity, resulting in a lower chloride-diffusion rate.
M4	Broad amorphous hump with minimal crystalline peaks and the lowest peak intensity.	Broad Al-O-Si asymmetric stretching bands are the dominant spectral feature.	The highly adhesive amorphous gel establishes continuous matrix links, although the limited crystalline content may reduce mechanical bonding.	The dense amorphous gel matrix acts as a barrier that limits chloride and moisture ingress.
M6	Distinct calcite diffraction peaks indicating carbonation.	Two carbonate absorption bands with strong absorption intensity.	The filler material increases matrix stiffness and confinement, whereas brittle interfaces may reduce ductility and bond strength.	Carbonation decreases pore-solution pH, removes the protective film on reinforcing steel, and may initiate corrosion damage.

5.3. Accelerated corrosion test

The accelerated corrosion test was used to assess the corrosion resistance of fiber-reinforced concrete by measuring reinforcement mass loss over time. The initial and final steel masses for mixes M1-M6 are presented in Table 4. The control mix M1 showed no mass loss during the first 45-90 min of testing. Reinforcement mass began to decrease after 120 min, indicating the onset of corrosion. The increasing mass loss over time suggests that microcracks and ionic-transport pathways developed, allowing chloride ions to enter and induce corrosion in plain HSC.

The addition of PPF reduced corrosion-related mass loss. Mix M2 showed significantly lower mass loss than the control mix, indicating improved corrosion resistance. Mix M3 also provided better corrosion protection than M1, although its performance was slightly lower than that of M2, possibly because the higher fiber content increased pore connectivity and reduced the uniformity of fiber dispersion. The HSFC mixes showed similar trends. M4 experienced moderate reinforcement mass loss after longer exposure, whereas the fiber-reinforced mixes M5 and M6 provided improved protection. M5 exhibited the lowest mass loss and therefore showed the best corrosion performance. Overall, the HSFC mixes demonstrated improved durability through enhanced resistance to environmental attack.

Some studies suggest that accelerated corrosion tests reproduce certain features of natural corrosion processes observed in the field. However, the applied DC voltage substantially increases the corrosion rate and does not fully represent chloride diffusion, moisture variation, and electrochemical-potential changes in real structures. Therefore, the data should be considered relative indicators of corrosion resistance rather than direct predictions of long-term service life. Future studies should include long-term natural-exposure tests and chloride-diffusion measurements to evaluate durability under realistic conditions.

5.4. Pull-out bond strength test

The peak bond stress of the HSC mixes increased from 13.61 MPa for M1 with 0% PPF to 14.15 MPa for M2 with 0.1% PPF and 14.32 MPa for M3 with 0.2% PPF. This improvement is attributed to the crack-bridging effect of PPF, which increases the tensile resistance of the concrete matrix and limits the development of microcracks from the reinforcing bar. The fibers provide additional confinement around the bar ribs, resulting in more effective mechanical interlock and higher bond resistance. They also help control splitting cracks, which commonly govern failure in pull-out tests of high-strength concrete.

The HSFC mixes showed a similar trend. Bond stress increased from 13.44 MPa for M4 with 0% PPF to 14.50 MPa for M5 with 0.1% PPF and 16.27 MPa for M6 with 0.2% PPF. The higher bond strength of the fiber-reinforced HSFC mixes may be attributed to improved particle packing and better consolidation, which enhance contact between the steel surface and the surrounding matrix. The combination of fiber reinforcement and flowable concrete produced a denser interfacial transition zone (ITZ), thereby improving resistance to radial cracking. The slip at peak bond stress increased with fiber content, from 0.65 mm in M1 to 1.29 mm in M6. These results indicate that fiber-reinforced mixes exhibit higher ductility and require greater energy for pull-out failure. PPF bridges cracks and allows stress transfer to continue through cracked regions, enabling the concrete matrix to sustain larger deformations before bond failure. Fig. 11 shows the pull-out test results.

Table 4. Accelerated corrosion test results.

M1			
Mix code	Time	Initial mass	Final mass
M1 - 1	(45 min)	0.195	0.195
M1 - 2	(60 min)	0.203	0.203
M1 - 3	(90 min)	0.177	0.177
M1 - 4	(120 min)	0.207	0.205
M1 - 5	(150 min)	0.179	0.176
M1 - 6	(180 min)	0.184	0.179
M2			
Mix code	Time	Initial mass	Final mass
M2 - 1	(45 min)	0.191	0.191
M2 - 2	(60 min)	0.204	0.204
M2 - 3	(90 min)	0.201	0.199
M2 - 4	(120 min)	0.196	0.195
M2 - 5	(150 min)	0.201	0.197
M2 - 6	(180 min)	0.205	0.201
M3			
Mix code	Time	Initial mass	Final mass
M3 - 1	(45 min)	0.205	0.205
M3 - 2	(60 min)	0.204	0.204
M3 - 3	(90 min)	0.203	0.202
M3 - 4	(120 min)	0.193	0.191
M3 - 5	(150 min)	0.203	0.199
M3 - 6	(180 min)	0.203	0.198

M4			
Mix code	Time	Initial mass	Final mass
M4 - 1	(45 min)	0.202	0.202
M4 - 2	(60 min)	0.192	0.192
M4 - 3	(90 min)	0.194	0.194
M4 - 4	(120 min)	0.206	0.204
M4 - 5	(150 min)	0.195	0.193
M4 - 6	(180 min)	0.194	0.191
M5			
Mix code	Time	Initial mass	Final mass
M5 - 1	(45 min)	0.195	0.195
M5 - 2	(60 min)	0.195	0.195
M5 - 3	(90 min)	0.205	0.205
M5 - 4	(120 min)	0.198	0.197
M5 - 5	(150 min)	0.207	0.204
M5 - 6	(180 min)	0.204	0.202
M6			
Mix code	Time	Initial mass	Final mass
M6 - 1	(45 min)	0.206	0.206
M6 - 2	(60 min)	0.205	0.205
M6 - 3	(90 min)	0.204	0.204
M6 - 4	(120 min)	0.205	0.203
M6 - 5	(150 min)	0.204	0.201
M6 - 6	(180 min)	0.204	0.202

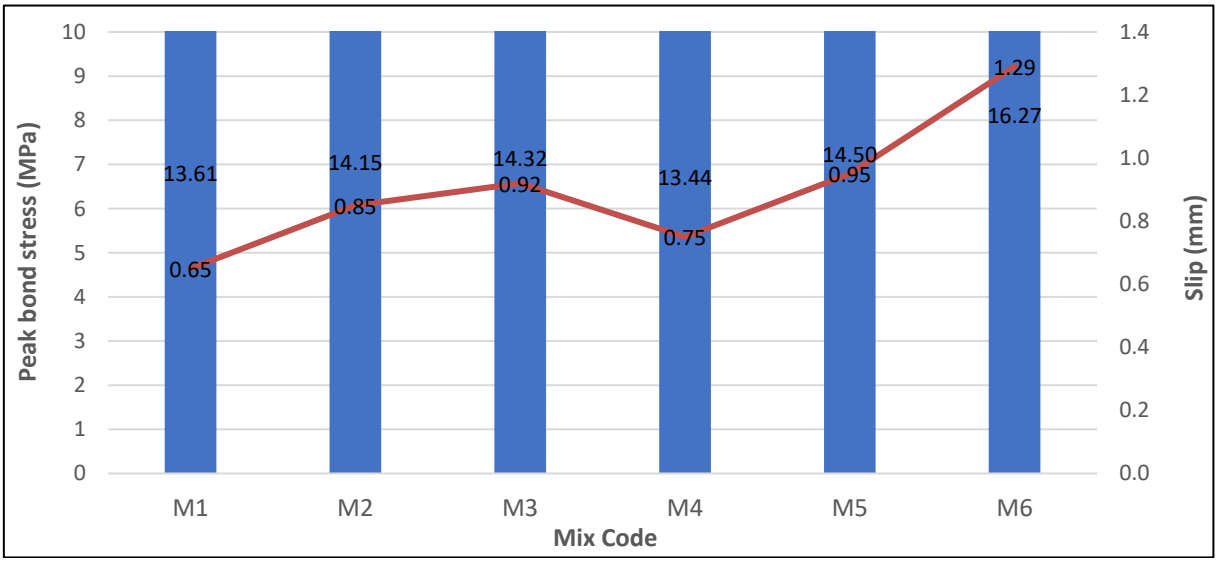

Fig. 11. Pull-out test results.

The experimental bond-strength values were higher than the values predicted by the design codes, as calculated using Eqs. (2) and (3). This difference is expected because the code equations are intended for safe design and include conservative assumptions. In addition, pull-out tests are conducted under controlled conditions, whereas structural members may also be affected by bending stresses, cracking, confinement variation, and other service conditions. Therefore, although the PPF-reinforced mixes showed improved bond performance, the results should be interpreted within the limitations of the test method.

The theoretical bond strength was evaluated according to BS 8110 (1997) and IS 456 (2000), and the results are tabulated in Table 5. According to BS 8110 (1997), the ultimate bond strength is expressed by Eq. (2).

$$f_{bu} = 0.50\sqrt{f_{cu}} \rightarrow f_{bu} = 0.50\sqrt{70} = 4.18 \text{ N/mm}^2 \quad (2)$$

where f_{bu} is the theoretical bond strength (N/mm^2), β is the bond coefficient (0.28 for plain bars and 0.50 for deformed bars), and f_{cu} is the cube compressive strength of concrete (N/mm^2).

According to IS 456:2000, the theoretical bond strength for plain bars is 1.9 N/mm^2. For deformed bars, this value is increased by 60%, as shown in Eq. (3).

$$\tau_{bd} = 1.9 \cdot 1.6 = 3.04 \text{ N/mm}^2 \quad (3)$$

Table 5. Bond strength test results.

Mix code	Peak stress (MPa)	Slip at peak (mm)	Stress at 0.25 mm slip	IS 456 design value	BS 8110 theoretical value
M1	13.61	0.65	5.44 MPa	3.04 MPa	4.18 MPa
M2	14.15	0.85	4.86 MPa	3.04 MPa	4.18 MPa
M3	14.32	0.92	4.42 MPa	3.04 MPa	4.18 MPa
M4	13.44	0.75	4.48 MPa	3.04 MPa	4.18 MPa
M5	14.50	0.95	3.31 MPa	3.04 MPa	4.18 MPa
M6	16.27	1.29	3.15 MPa	3.04 MPa	4.18 MPa

6. Conclusions

This experimental investigation examined the influence of PPF on the mechanical properties, bond behavior, corrosion resistance, and microstructural characteristics of HSC and HSFC. The main conclusions are as follows:

- Overall, the results showed that adding PPF had a negligible effect on compressive strength, with a variation of approximately ±3%, while notable improvements were observed in tensile and flexural strengths. The increase in splitting tensile strength ranged from 10% to 18% at 0.1% PPF, and flexural strength increased by 8% to 12%.
- The optimum fiber content was 0.1% by volume. Although 0.2% PPF improved tensile and bond properties, the additional benefits were limited, possibly because of fiber agglomeration.
- Pull-out test results indicated that adding fibers improved the bond between reinforcing bars and concrete. Bond strength increased from 13.61 MPa for M1 to 14.32 MPa for M3 and 16.27 MPa for M6. This improvement resulted from crack bridging and enhanced protection against splitting around the reinforcing bars, which improved mechanical interlocking.
- HSFC showed superior mechanical properties and bond strength compared with HSC. Improved particle arrangement and more uniform fiber distribution enhanced workability and produced a denser interfacial transition zone (ITZ).
- Steel mass loss during accelerated corrosion testing was lower in the fiber-reinforced mixes, whereas the control specimens exhibited earlier crack development. The fiber-reinforced system therefore provided better corrosion protection by reducing crack size and crack number and by limiting chloride ingress through a more resistant pore structure.
- XRD and FTIR analyses revealed the formation and development of hydration products such as C-S-H gel, ettringite, and calcite, as well as ongoing densification of the cement matrix over time. These results also indicated improved mechanical and long-term performance of the fiber-reinforced mixes owing to enhanced silicate polymerization and microstructural development.
- The measured bond strengths exceeded the predictions of IS 456:2000 and BS 8110, suggesting that current code provisions are conservative for fiber-reinforced high-strength concrete systems.
- The findings demonstrate that PPF-reinforced HSFC provides a balanced combination of strength, bond improvement, and durability, making it a suitable material for reinforced concrete structures exposed to aggressive environments.

Acknowledgements

The authors would like to thank MSRIT, Bengaluru for their support and contribution to this study.

Funding

The authors received no financial support for the research, authorship, and/or publication of this manuscript.

Conflict of Interest

The authors declare(s) no potential conflicts of interest with respect to the research, authorship, and/or publication of this manuscript.

Data Availability

The datasets generated and/or analyzed during the current study are not publicly available but are available from the corresponding author upon reasonable request.

AI Assistance

During the preparation of this manuscript, Grammarly, Gemini and ChatGPT were used exclusively for language editing and stylistic refinement. The authors take full responsibility for the content, interpretation, and conclusions of the published article.

Author Contributions

All authors made substantial contributions to the conception and design of the study, acquisition of data, analysis and interpretation of data; drafted or critically revised the manuscript for important intellectual content; and approved the final version to be published.

References

Abdraimov I (2024). Strength and durability effect of self-compacting concrete reinforcement with micro-silica and volume fiber. *International Journal of GEOMATE*, 27(119), 1-8.

Aguirre-Guerrero AM, Robayo-Salazar RA, Mejía De Gutiérrez R (2021). Corrosion resistance of alkali-activated binary reinforced concrete based on natural volcanic pozzolan exposed to chlorides. *Journal of Building Engineering*, 33, 101593.

Ahmed TW, Aljubory NH, Zidan RS (2021). Properties and performance of polypropylene fiber reinforced concrete: A review. *Tikrit Journal of Engineering Sciences*, 27(2), 82-97.

Al-Safi S, Altharehi A, Alameri IA, Al-Jolahy A (2025). The mechanical properties of cement mortar reinforced with silica fume subjected to sulfate and chloride environment. *Challenge Journal of Structural Mechanics*, 11(1), 55–69.

ASTM C1585 (2020). Standard test method for measurement of rate of absorption of water by hydraulic-cement concretes. ASTM International, West Conshohocken, PA, USA.

Bajić P, Leporace-Guimil B, Andrade C, Tošić N, De La Fuente A (2025). Chloride-induced corrosion effects on the structural performance of concrete with rebar and fibres: A review. *Applied Sciences*, 15(12), 6457.

Bakhita CD, Kanali C, Onchiri RO (2025). Mechanical properties of high-strength concrete reinforced with basalt and polypropylene fibers. *Engineering, Technology & Applied Science Research*, 15(3), 22725-22733.

BS 8110 (1997). Structural use of concrete. Part 1: Code of practice for design and construction. British Standards Institution, London, UK.

Burdziński M, Niedostatkiewicz M (2022). Experimental-numerical analysis of the effect of bar diameter on bond in pull-out test. *Buildings*, 12(9), 1392.

Chen Y, Waheed MS, Iqbal S, Rizwan M, Room S (2024). Durability properties of macro-polypropylene fiber reinforced self-compacting concrete. *Materials*, 17(2), 284.

De Alencar Monteiro VM, Lima LR, De Andrade Silva F (2018). On the mechanical behavior of polypropylene, steel and hybrid fiber reinforced self-consolidating concrete. *Construction and Building Materials*, 188, 280-291.

Deng Y, Yang Y (2024). An experimental study on corrosion resistance and bond behavior of reinforced concrete structures with various fibers. *KSCE Journal of Civil Engineering*, 28(12), 5593-5603.

Diab AM, Elyamany HE, Hussein MA, Al Ashy HM (2014). Properties of pull-out bond strength and concept to assess ultimate bond stress of NSC and HSC. *Magazine of Concrete Research*, 66(17), 877-895.

Dubal AC, Naktode PL (2024). Effect of polypropylene fiber on the properties of self-compacting concrete with M-sand. *Educational Administration Theory and Practice*, 30(2), 1-8.

Fahmy NG, Hussien RM, Abd El-Hafez LM, Mohamed RAS, Faried AS (2022). Comparative study on fresh, mechanical, microstructure properties and corrosion resistance of self-compacted concrete incorporating nanoparticles extracted from industrial wastes under various curing conditions. *Journal of Building Engineering*, 57, 104874.

Faraj RH, Sherwani AFH, Daraei A (2019). Mechanical, fracture and durability properties of self-compacting high-strength concrete containing recycled polypropylene plastic particles. *Journal of Building Engineering*, 25, 100808.

Hadi MNS (2008). Bond of high strength concrete with high strength reinforcing steel. *The Open Civil Engineering Journal*, 2(1), 143-147.

Hasan M, Alkhaly YR, Hamzani, Fikri R, Saidi T (2025). Properties of high-strength concrete incorporating calcined diatomaceous earth, polypropylene and glass fibers. *Buildings*, 15(2), 225.

Hima Bindu K, Rathna Chary M, Haranatti JS, Rao LV, Dev PV, Kotov EV (2024). Behavior of high strength reinforced cement concrete with polypropylene and steel fibres. *MATEC Web of Conferences*, 392, 01011.

Hou L, Zhou B, Guo S, Aslani F, Chen D (2019). Corrosion behavior and flexural performance of reinforced concrete/ultrahigh toughness cementitious composite beams under sustained loading and shrinkage cracking. *Construction and Building Materials*, 198, 278-287.

IS 456 (2000). Plain and reinforced concrete. Code of practice. Bureau of Indian Standards, New Delhi, India.

IS 516 (1959). Methods of tests for strength of concrete. Bureau of Indian Standards, New Delhi, India.

IS 2770 (1967). Methods of testing bond in reinforced concrete. Part 1: Pull-out test. Bureau of Indian Standards, New Delhi, India.

IS 5816 (1999). Method of test for splitting tensile strength of concrete. Bureau of Indian Standards, New Delhi, India.

IS 10262 (2019). Concrete mix proportioning. Guidelines. Bureau of Indian Standards, New Delhi, India.

IS 12269 (2013). Ordinary Portland cement, 53 grade. Specification. Bureau of Indian Standards, New Delhi, India.

Khaloo A, Daneshyar A, Rezaei B, Fartash A (2022). Fiber bridging in polypropylene-reinforced high-strength concrete: An experimental and numerical survey. *Structural Concrete*, 23(1), 457-472.

Labaran YH, Atmaca N, Tan M, Atmaca K (2024). High-strength fiber-reinforced concrete: Assessing the impact of polyvinyl alcohol, glass and polypropylene fibers on structural integrity and cost efficiency. *Discover Civil Engineering*, 1(1), 37.

Leporace-Guimil B, Conforti A, Zerbino R, Plizzari GA (2021). Chloride-induced corrosion in reinforced concrete and fiber reinforced concrete elements under tensile service loads. *Cement and Concrete Composites*, 124, 104245.

Lin JX, Luo RH, Su JY, Guo YC, Chen WS (2024). Coarse synthetic fibers as a replacement to steel fibers in UHPC: Tensile behavior, environmental and economic assessment. *Construction and Building Materials*, 412, 134654.

Mazaheripour H, Ghanbarpour S, Mirmoradi SH, Hosseinpour I (2011). The effect of polypropylene fibers on the properties of fresh and hardened lightweight self-compacting concrete. *Construction and Building Materials*, 25(1), 351-358.

Mohamad N, Embong R, Othman NH, Muthusamy K, Jaafar MFM (2025). Flowability and compressive strength of ternary blended cement mortar of coal bottom ash and ground cockle shell ash. *Challenge Journal of Concrete Research Letters*, 16(1), 25–32.

Ouda AS (2024). Insights into the physico-mechanical characteristics and corrosion behavior of high-performance heavy density concrete used in the construction of electro-nuclear power facilities. *Construction and Building Materials*, 443, 137838.

Pan C, Chen N, He J, Liu S, Chen K, Wang P, Xu P (2020). Effects of corrosion inhibitor and functional components on the electrochemical and mechanical properties of concrete subject to chloride environment. *Construction and Building Materials*, 260, 119724.

Patil SV (2025). Predictive modelling of acoustic emission signal data for corrosion assessment: A modified dimensional analysis based approach. *Challenge Journal of Concrete Research Letters*, 16(3), 125–132.

Qin Y, Zhang X, Chai J, Xu Z, Li S (2019). Experimental study of compressive behavior of polypropylene-fiber-reinforced and polypropylene-fiber-fabric-reinforced concrete. *Construction and Building Materials*, 194, 216-225.

Ranjbar N, Talebian S, Mehrali M, Kuenzel C, Metselaar HSC, Jumaat MZ (2016). Mechanisms of interfacial bond in steel and polypropylene fiber reinforced geopolymer composites. *Composites Science and Technology*, 122, 73-81.

Resende HF, Reis ED, Arroyo FN, De Moraes MHM, Dos Santos HF, Da Silva EG, Lahr FAR (2022). Residual mechanical properties and durability of high-strength concrete with polypropylene fibers in high temperatures. *Materials*, 15(13), 4711.

Sangkeaw P, Thongchom C, Keawsawasvong S, Prasittisopin L (2025). Mechanical properties and microstructure of cellulose fiber and synthetic fiber reinforced high-strength concrete. *Arabian Journal for Science and Engineering*, 50(3), 2149-2168.

Sola E, Ožbolt J, Balabanić G, Mir ZM (2019). Experimental and numerical study of accelerated corrosion of steel reinforcement in concrete: Transport of corrosion products. *Cement and Concrete Research*, 120, 119-131.

Song HW, Saraswathy V (2007). Corrosion monitoring of reinforced concrete structures: A review. *International Journal of Electrochemical Science*, 2(1), 1-28.

Srivastava A, Mishra A, Singh SK (2025). Mechanical and durability study of nano TiO2 and nano SiO2 on fiber reinforced concrete. *Challenge Journal of Concrete Research Letters*, 16(1), 33–39.

Tanash AO, Budiea AMA, Md Jaafar MF, Muthusamy K, Zulkarnain F (2025). Experimental study on the mechanical performance of polypropylene fiber-reinforced concrete incorporating palm oil fuel ash as partial cement replacement. *Challenge Journal of Concrete Research Letters*, 16(3), 115–124.

Tarhan Y, Tarhan İH, Perrot A (2025). Improving bond performance of 3D-printable earth-based mortar reinforced with jute fibers. *Challenge Journal of Structural Mechanics*, 11(2), 99–105.

Tastani SP, Pantazopoulou SJ (2010). Direct tension pullout bond test: Experimental results. *Journal of Structural Engineering*, 136(6), 731-743.

Torre-Casanova A, Jason L, Davenne L, Pinelli X (2013). Confinement effects on the steel-concrete bond strength and pull-out failure. *Engineering Fracture Mechanics*, 97, 92-104.

Torres-Ortega R, Quiñonez-Bolaños E, Tejada-Tovar C, García-Díaz Y, Cabarcas-Torres I (2021). High-strength concrete with natural aggregates, silica fume and polypropylene macrofibers. *Ciencia e Ingeniería Neogranadina*, 31(2), 27-40.

Touahri A, Branci T, Yahia A, Ezziane K (2021). Effect of recycled polypropylene fiber on high strength concrete and normal strength concrete properties. *Advances in Materials Research*, 10(4), 267-281.

Tsiotsias K, Pantazopoulou SJ (2021). Bond behavior of high-performance fiber reinforced concrete under direct tension pullout. *Engineering Structures*, 243, 112701.

Urtekin Y, Çelik Z (2025). Investigation of the effects of re-curing on mechanical properties of basalt-polypropylene hybrid fiber concretes after exposure to high temperature. *Challenge Journal of Structural Mechanics*, 11(1), 14–23.

Uysal M, Tanyildizi H (2012). Estimation of compressive strength of self-compacting concrete containing polypropylene fiber and mineral additives exposed to high temperature using artificial neural network. *Construction and Building Materials*, 27(1), 404-414.

Varghese A, Anand N, Arulraj GP, Alengaram UJ (2019). Influence of fibers on bond strength of concrete exposed to elevated temperature. *Journal of Adhesion Science and Technology*, 33(14), 1521-1543.

Zhao J, Yang X, Fan J, Gao S, Ma H (2022). Research on dynamic compressive performance of polypropylene fiber reinforced high-strength concrete under freeze-thaw environment. *Advances in Materials Science and Engineering*, 2022, 9079019.